catalysts

MDPI

Article

A Highly Efficient Bifunctional Catalyst CoO_x/tri-g-C_3N_4 for One-Pot Aerobic Oxidation–Knoevenagel Condensation Reaction

Jiequn Wu, Weiming Hua, Yinghong Yue * and Zi Gao

Department of Chemistry, Shanghai Key Laboratory of Molecular Catalysis and Innovative Materials, Fudan University, Shanghai 200438, China; jiequnw@163.com (J.W.); wmhua@fudan.edu.cn (W.H.); zigao@fudan.edu.cn (Z.G.)

* Correspondence: yhyue@fudan.edu.cn; Tel.: +86-21-3124-9120

Received: 13 June 2020; Accepted: 23 June 2020; Published: 25 June 2020

Abstract: A highly efficient bifunctional catalyst of an s-triazine-based carbon-nitride-supported cobalt oxide is developed for the aerobic oxidation–Knoevenagel condensation tandem reaction of benzyl alcohol and malononitrile, whereby 96.4% benzyl alcohol conversion with nearly 100% selectivity towards benzylmalononitrile can be obtained in 6 h at 80 °C. The excellent catalytic performance derives from the high basicity of carbon nitride and strong redox ability of Co species induced by carbon nitride. The catalyst is also quite stable and can be reused without any regeneration treatment, whose product yield is only an 11.5% reduction after four runs.

Keywords: one-pot reaction; aerobic oxidation; Knoevenagel condensation; cobalt oxide; carbon nitride

1. Introduction

The development of alternative clean and efficient processes is one of the priorities for modern chemistry, since traditional chemical synthesis and the resulting large consumption of fossil energy have caused a series of environmental pollution problems, which are destroying our ecological environment. The one-pot procedure has raised extensive interest since it can simplify the synthetic routes and minimize the production waste and energy consumption [1–5]. The challenges for one-pot transformation involve the development of heterogeneous catalysts with different catalytically active sites that can promote different reactions simultaneously and independently while not interfering with each other [6–8].

Benzylmalononitrile is a key intermediate for the preparation of antimalarial, which has numerous applications in the fields of pharmaceutical, biological, and synthetic chemistry [9]. Benzylmalononitrile is traditionally prepared by Knoevenagel condensation of malononitrile and benzaldehyde, the latter of which is generally obtained from the selective oxidation of benzyl alcohol, since alcohol is readily available as compared with the corresponding aldehydes. Preparation of benzylmalononitrile through tandem aerobic oxidation–Knoevenagel condensation reaction can greatly improve the synthesis efficiency [10–15]. One-pot synthesis of the above tandem reaction has been achieved by several researchers, including Qi [16], Miao [17], and Yan [18]. However, developing a simple and efficient catalyst is still a big challenge, since the activation of molecular oxygen under mild conditions is very difficult, especially without a noble metal.

Graphitic carbon nitride is known as a solid base catalyst that is active for the Knoevenagel condensation of benzaldehyde and malononitrile [19–22]. Meanwhile, it is also an outstanding support for the transition metal oxides, since the redox catalytic ability of the oxides can be improved greatly due to their unique interaction with g-C_3N_4 [23–27]. Recently, s-triazine-based carbon

nitride (tri-g-C_3N_4) has been found to be a more ideal solid base catalytic material than g-C_3N_4 because it has more uncondensed amino groups (-NH, -NH_2) in the structure as compared with g-C_3N_4 [27–31]. These uncondensed amino groups can also be employed as anchors for supporting transition metal oxides.

Herein, a bifunctional catalyst with both basic and redox properties has been designed by supporting CoO_x on tri-g-C_3N_4. Due to the basic activity of tri-g-C_3N_4 and the enhanced redox ability of Co species, this catalyst has excellent catalytic activity in aerobic oxidation–Knoevenagel condensation tandem reaction of benzyl alcohol and malononitrile, without addition of any auxiliary reagents. The reasons for this remarkable catalytic activity of CoO_x/tri-g-C_3N_4 are also elucidated.

2. Results and Discussion

2.1. Catalyst Characterization

Figure 1 shows XRD patterns of CoO_x/tri-g-C_3N_4 with different CoO_x contents, together with that of tri-g-C_3N_4. For tri-g-C_3N_4, in addition to the two diffraction peaks assigned to g-C_3N_4 with 2θ of 13.2° and 27.7°, peaks at 12.3°, 20.0°, 24.0º, 26.7°, 29.5°, and 32.2° can also be observed, which are ascribed to tri-g-C_3N_4, corresponding to its (100), (110), (200), (002), (102), and (210) crystal planes, respectively [32]. The characteristic diffractions of g-C_3N_4 decrease and later disappear, while the (100) and (002) diffractions of tri-g-C_3N_4 remain with the increase of CoO_x loading, demonstrating the transformation of g-C_3N_4 to tri-g-C_3N_4. No obvious characteristic diffraction peak of CoO_x can be identified due to the relatively small CoO_x loading and its high dispersion.

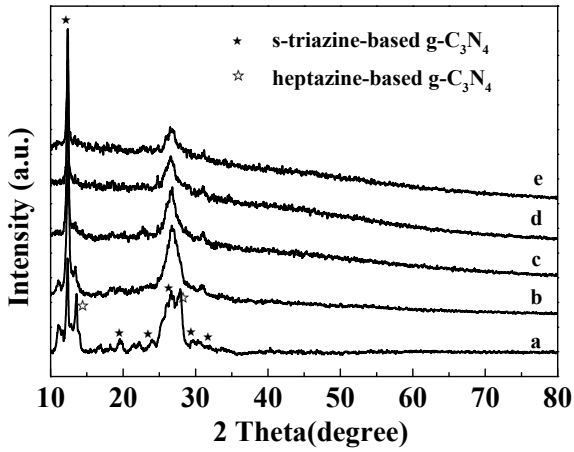

Figure 1. The XRD patterns of (**a**) tri-g-C_3N_4, (**b**) 1CoO_x/tri-g-C_3N_4, (**c**) 3CoO_x/tri-g-C_3N_4, (**d**) 5CoO_x/tri-g-C_3N_4, and (**e**) 7CoO_x/tri-g-C_3N_4.

The generation of the tri-g-C_3N_4 structure was further confirmed by the FT-IR spectra, which is shown in Figure 2. An intense absorption peak at 808 cm^{-1} corresponding to the breathing modes of the s-triazine units [32] can be observed for all the catalysts. Skeletal stretching vibrations together with bending vibrations of s-triazine or tri-s-trizaine located at 1250~1700 cm^{-1} also appeared in the spectra. The broad absorption band in the range of 3100~3300 cm^{-1} belongs to the stretching vibration of uncondensed N–H. A significant shift of the N–H band can be detected, probably caused by the interaction between the N–H group and CoO_x species.

The SEM images of the obtained catalysts are presented in Figure 3, where tri-g-C_3N_4 exhibits a block structure made up of irregular layered sheets. No clear differences in morphology were found after CoO_x loading, signifying that CoO_x did not destroy the tri-g-C_3N_4 structure. This was confirmed by N_2 adsorption measurements, with similar type III isotherms with H3 hysteresis loops shown for all of the catalysts (illustrated in Figure S1). The hysteresis loops are more evident for the supported catalysts, revealing the increase of interparticle voids after the CoO_x support. Table 1 shows the specific

surface areas and total pore volumes of the catalysts. Both become larger after Co loading, probably due to the intercalation of Co species into the layered structure, resulting in more interparticle voids. However, when the Co loading is further increased, the pore channel of tri-g-C_3N_4 may be partially blocked, leading to a reduction in pore volume.

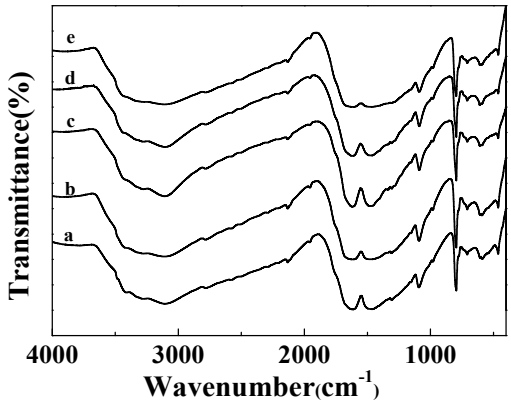

Figure 2. FT-IR spectra of (**a**) tri-g-C_3N_4, (**b**) 1CoO_x/tri-g-C_3N_4, (**c**) 3CoO_x/tri-g-C_3N_4, (**d**) 5CoO_x/tri-g-C_3N_4, and (**e**) 7CoO_x/tri-g-C_3N_4.

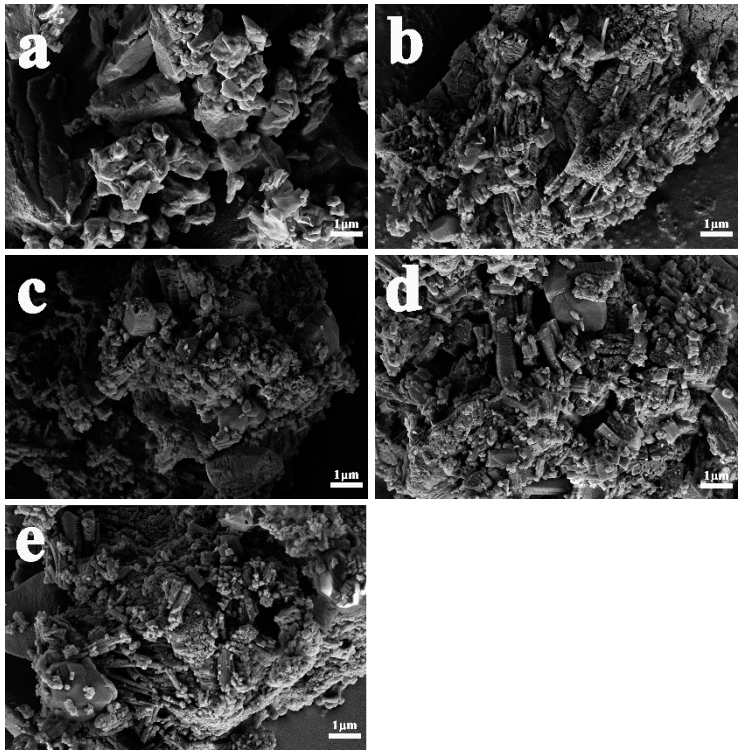

Figure 3. SEM images of (**a**) tri-g-C_3N_4, (**b**) 1CoO_x/tri-g-C_3N_4, (**c**) 3CoO_x/tri-g-C_3N_4, (**d**) 5CoO_x/tri-g-C_3N_4, and (**e**) 7CoO_x/tri-g-C_3N_4.

The thermogravimetric method was employed to analyze the thermal stability of CoO_x/tri-g-C_3N_4 catalysts in air atmosphere. The results are shown in Figure 4. CoO_x/tri-g-C_3N_4 catalysts are all stable below 400 °C; only a slight weight loss caused by the desorption of H_2O or CO_2 was observed at the temperature range of 20–200 °C. The thermal decomposition temperature decreased gradually with the CoO_x loadings, indicating that their thermal stability was lowered by the Co loadings. The actual content of Co in the catalyst was calculated by the remaining weight after TGA experiments. As shown

in Table 1, these were quite close to the contents added. The slightly increased content was caused by the partial decomposition of the tri-g-C_3N_4 support during the final calcination.

Table 1. Textural and basic properties of tri-g-C_3N_4 and CoO_x/tri-g-C_3N_4.

Catalysts	S_{BET} (m^2/g)	V_{total} (cm^3/g)	Pore Size (nm) [a]	Co Content (%) [b]	Amount of Base Sites (mmol/g) [c]
tri-g-C_3N_4	3	0.02	26.3	–	3.25
1CoO_x/tri-g-C_3N_4	13	0.12	35.9	1.3	2.73
3CoO_x/tri-g-C_3N_4	13	0.13	37.9	2.9	2.62
5CoO_x/tri-g-C_3N_4	9	0.07	32.3	5.4	2.50
7CoO_x/tri-g-C_3N_4	12	0.10	32.2	7.6	2.40

[a] Defined as $4V_{total}/S_{BET}$; [b] Weight percentage of Co obtained by thermogravimetric analysis (TGA); [c] obtained by neutralization titration.

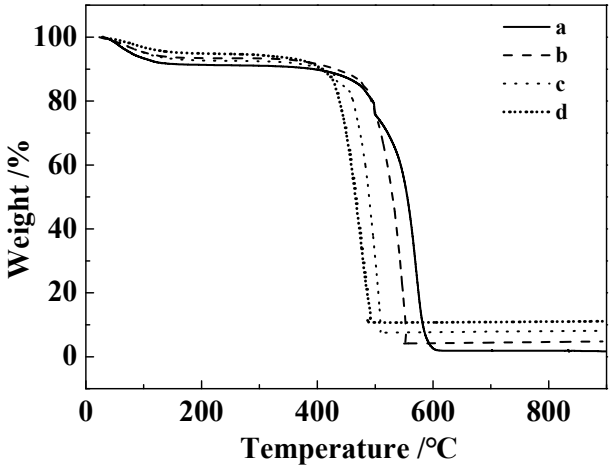

Figure 4. TG thermograms of (**a**) 1CoO_x/tri-g-C_3N_4, (**b**) 3CoO_x/tri-g-C_3N_4, (**c**) 5CoO_x/tri-g-C_3N_4, and (**d**) 7CoO_x/tri-g-C_3N_4.

The XPS method was used to detect the chemical states of Co and O on the catalyst surface, the results of which are displayed in Figures S2 and S3. Two peaks at ~796 eV and ~780 eV appeared in Figure S2, which are attributed to the Co $2p_{1/2}$ and Co $2p_{3/2}$ spin orbits, respectively. The ~780 eV peak can be deconvoluted into two peaks, with peak positions of 780.8 eV and 782.2 eV, corresponding to Co^{3+} and Co^{2+} species, respectively [26,33,34]. The Co^{3+}/Co^{2+} ratio after fitting is listed in Table 2. It can be clearly seen that the ratio increases initially with the increase of Co loading. After further increasing the loading of Co, the Co^{3+}/Co^{2+} ratio decreases. When the Co loading reaches 5%, the Co^{3+}/Co^{2+} ratio is the largest. A high concentration of Co^{3+} may lead to an increase in the number of chemically adsorbed oxygen species on the catalyst surface [27]. This is proven by the O_{1s} spectra illustrated in Figure S3, which can be fitted into two peaks, with peak positions of 532.5 eV and 531.5 eV, corresponding to the adsorbed oxygen species and surface lattice oxygen species, respectively [35,36]. The ratio of the adsorbed oxygen species to the surface lattice oxygen ones has the same change tendency as the ratio of Co^{3+} to Co^{2+}. The surface-adsorbed oxygen (O_{ads}) is usually located in surface defects and is easier to reduce [37–39], which is crucial for catalytic oxidation.

Table 2. XPS results of CoO_x/tri-g-C_3N_4 catalysts.

Catalysts	Co $2p_{3/2}$ Peaks			O_{1S} Peaks		
	Co^{2+} (eV)	Co^{3+} (eV)	Co^{3+}/Co^{2+}	O_{ads} (eV)	O_{latt} (eV)	O_{ads}/O_{latt}
1CoO_x/tri-g-C_3N_4	782.4	780.8	0.60	532.4	531.2	0.46
3CoO_x/tri-g-C_3N_4	782.2	780.8	0.84	532.8	531.5	0.60
5CoO_x/tri-g-C_3N_4	782.4	780.8	1.63	532.9	531.7	1.11
7CoO_x/tri-g-C_3N_4	782.4	780.8	1.31	532.8	531.6	0.84

The surface basicities of the catalysts were measured by acid–base neutralization titration in aqueous solution, since the reactions investigated here are carried out in the liquid phase. The results are shown in Table 1. A large amount of basic sites were detected on tri-g-C_3N_4 surface despite its small specific surface area. This was because of the swelling effects in the liquid phase, which was also found on sulfonated carbon catalysts [40]. The amount of basic sites decreased with the Co loadings due to the interaction between the N-H group and CoO_x species. However, the reduction was not too big in the range of present CoO_x content. Basic sites measuring 2.40 mmol/g still remained on the 7CoO_x/tri-g-C_3N_4 catalyst, which was larger than those on pristine g-C_3N_4 [19].

2.2. Catalytic Performance

2.2.1. Aerobic Oxidation of Benzyl Alcohol

Aerobic oxidation of benzyl alcohol was conducted over CoO_x/tri-g-C_3N_4 catalysts, as well as tri-g-C_3N_4. The results are listed in Table 3. It can be seen that tri-g-C_3N_4 is not active for the oxidation, indicating that redox active sites come from the supported CoO_x species. The activity increased sharply with the CoO_x loadings, reaching the maximum and then decreasing slowly with further increases of the amount of CoO_x. 5CoO_x/tri-g-C_3N_4 has the best activity. The excellent redox catalytic ability can be attributed to the high chemisorbed oxygen species on the surface, since they are thought to be the most active oxygen species in the oxidation reaction, which can promote the formation of oxygen vacancies, as well as enhance the exchange of gaseous oxygen molecules and adsorbed oxygen molecules on the catalyst surface, thus promoting the oxidation reaction [41–43]. This can be proven by the XPS results in Table 2, which indicate that the change in activity with the Co loadings has the same trend as in the adsorbed oxygen-to-lattice oxygen ratio (O_{ads}/O_{latt}).

Table 3. Catalyst activity of aerobic oxidation and Knoevenagel condensation.

Catalysts	Aerobic Oxidation		Knoevenagel Condensation	
	Time (h)	Conversion (%)	Time (h)	Conversion (%)
tri-g-C_3N_4	3.0	2.0	0.5	76
1CoO_x/tri-g-C_3N_4	3.0	49.9	0.5	74
3CoO_x/tri-g-C_3N_4	3.0	63.0	0.5	72
5CoO_x/tri-g-C_3N_4	3.0	87.6	0.5	71
7CoO_x/tri-g-C_3N_4	3.0	79.3	0.5	70

2.2.2. Knoevenagel Condensation of Benzaldehyde and Malononitrile

The catalytic activities of the CoO_x/tri-g-C_3N_4 catalysts for the Knoevenagel condensation of benzaldehyde and malononitrile were also evaluated, together with that of tri-g-C_3N_4. All were very active for the condensation; nearly 100% conversion of benzaldehyde was obtained with the same reaction condition as oxidation (80 °C, 3 h). This can be ascribed to the abundant uncondensed amino groups (–NH, –NH_2) in the structure of tri-g-C_3N_4. Table 3 summarizes their catalytic activities at the lower temperature of 60 °C. It can be seen that the activity decreased with the CoO_x loading, which can be ascribed to the reduction of basic sites, since Knoevenagel condensation is a typical base-catalyzed reaction. However, the decrease in activity is not as evident. The possible reason is that the reduction of basic sites was small, resulting in sufficient active sites remaining for catalyzing Knoevenagel condensation.

2.2.3. Oxidation–Condensation Tandem Reaction

The catalytic performances of CoO_x/tri-g-C_3N_4 catalysts towards one-pot aerobic oxidation–Knoevenagel condensation tandem reaction were evaluated, the results of which are summarized in Table 4. All were active for the tandem reaction. It can be seen that the conversion of benzyl alcohol increases with the CoO_x loading, reaches the maximum at 5CoO_x/tri-g-C_3N_4, then

decreases with further increases of the CoO_x content. The trend for activity is exactly the same as that of the oxidation reaction, owing to the much faster rate of condensation as compared with that of oxidation. No intermediates benzaldehyde were found in any cases, indicating the oxidation is the rate-determined step. The benzyl alcohol conversion also increased with the reaction time, and 96.4% yield of benzylmalononitrile was obtained in 6 h over $5CoO_x$/tri-g-C_3N_4. The excellent catalytic performance could be due to its dual function—the redox ability of supported CoO_x species combined with the basic sites retained in the tri-g-C_3N_4 support, which was confirmed by the above results of individual oxidation and condensation reactions.

Table 4. Catalyst activity of tandem aerobic oxidation–Knoevenagel condensation reaction.

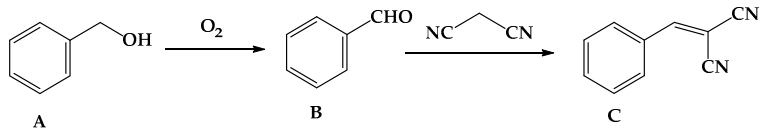

Catalysts	Time (h)	Conversion of A (%)	Yield of C (%)
tri-g-C_3N_4	6	2.1	1.9
$1CoO_x$/tri-g-C_3N_4	3	43.9	43.9
	6	65.5	65.5
$3CoO_x$/tri-g-C_3N_4	3	53.7	53.7
	6	85.5	85.5
$5CoO_x$/tri-g-C_3N_4	3	83.2	83.2
	6	96.4	96.4
$7CoO_x$/tri-g-C_3N_4	3	65.1	65.1
	6	90.7	90.7

It can also be seen that the conversion in individual oxidation over $5CoO_x$/tri-g-C_3N_4 at 3 h (87.6%) is very close to that in the tandem reaction (83.2%), indicating that the two types of active sites in $5CoO_x$/tri-g-C_3N_4 would not interfere with each other during the tandem reaction.

The reusability of $5CoO_x$/tri-g-C_3N_4 in the aerobic oxidation–Knoevenagel condensation tandem reaction was also investigated. After the reaction, the catalyst was filtered out from the reaction liquid and then dried for the repeatability test. The results are shown in Figure 5. The conversion of benzyl alcohol decreased continuously but slowly from 96.4% to 84.9% after three regeneration processes, while the selectivity remained intact, indicating that $5CoO_x$/tri-g-C_3N_4 is quite stable in the liquid-phase tandem reactions.

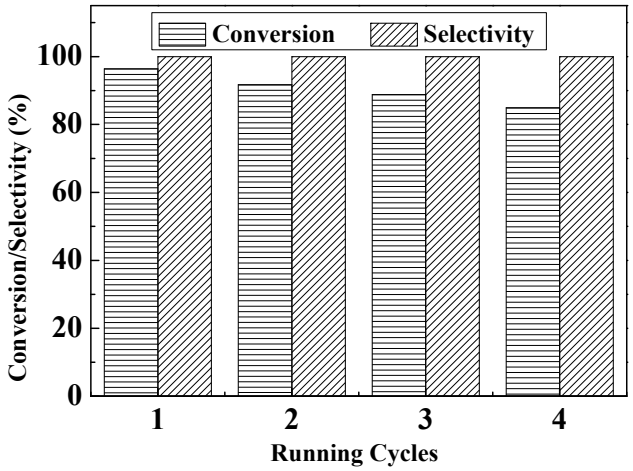

Figure 5. Recycling of $5CoO_x$/tri-g-C_3N_4 catalyst in the aerobic oxidation–Knoevenagel condensation tandem reaction.

Table 5 summarizes the catalytic behavior over various catalysts for this tandem aerobic oxidation–Knoevenagel condensation reaction, which has been reported in previous literature. The high yield of benzylmalononitrile was obtained over our present catalyst under mild reaction conditions, without the use of expensive noble metals, giving it advantages over most of the catalysts reported before. Since Co_3O_4/C_3N_4 composites are active for aerobic oxidation of various aromatic alcohols bearing either electron-withdrawing groups or electron-donating groups [27], the present catalyst is believed to be applicable for aerobic oxidation–Knoevenagel condensation of various aromatic alcohols besides benzyl alcohol.

Table 5. Summary of the activities for tandem oxidation–condensation reaction over various catalysts.

Catalyst	Oxidant	Temperature (°C)	Time (h) [a]	Conversion (%)	Yield (%)	Ref.
Au@Cu(II)-MOF	Air	110	15 + 7	99	99	[10]
OMS-2-SF	O_2	85	9 + 0.5	99.5	84.5	[11]
Pd/LS-AT-OH^-	O_2	85	9 + 2	89.6	88.3	[12]
Pd_1-Au_1/LDH	O_2	80	1.5 + 1	99	98.0	[13]
UiO-66-Ru	O_2	100	1 + 5	100	89.3	[14]
Pd/COF-TpPa-Py	O_2	80	4 + 1.5	98	98	[15]
Au@MIL-53(NH_2)	O_2	100	13	99	99	[16]
Cu_3TATAT-3	O_2	75	12	95	95	[17]
Fe_3O_4@SiO_2@PEI@Ru$(OH)_x$	O_2	110	22	98.6	90.2	[18]
5CoO_x/tri-g-C_3N_4	O_2	80	6	96.4	96.4	Present work

Note: [a] "*m* + *n*" means step-by-step reaction without separation of intermediate benzaldehyde.

3. Materials and Methods

3.1. Catalyst Preparation

The s-triazine-based g-C_3N_4 was synthesized as follows: 5 g melamine was dispersed in 30 mL ethylene glycol to obtain a saturated solution. Hereafter, 60 mL 0.1 M HNO_3 solution was added and stirred for 1 h at room temperature. The resulting mixture was filtered and washed three times with ethanol to remove the remaining nitric acid and ethylene glycol. Afterward, the mixture was dried at 120 °C and put into a covered ceramic crucible, heated under air flow at 5 °C/min up to 400 °C, and maintained for 2 h. The resulting product was cooled and grounded into powder.

The tri-g-C_3N_4 supported CoO_x catalysts were synthesized as follows: 1 g obtained tri-g-C_3N_4 was put into an aqueous solution with a calculated content of $Co(NO_3)_2$ $6H_2O$. The mixture was stirred for 1 h at room temperature. After drying at 120 °C, the resulting solid was calcined under air flow at 2 °C/min up to 300 °C and maintained for 3 h. The obtained product was designated as *y*CoO_x/tri-g-C_3N_4, where *y* stands for the weight percentage of Co added.

3.2. Characterization of Catalyst

X-ray diffraction (XRD) was carried out on a D2 PHASER X-ray diffractometer (Brucker, Madison, WI, USA) using nickel-filtered Cu-K_α (λ = 0.15418 nm) at 40 kV and 30 mA in the range of 10°–80°. Fourier transform infrared spectra (FT-IR) were measured on a Nicolet iS10 spectrometer (ThermoFisher, Waltham, MA, USA). Scanning electron microscopy (SEM) was recorded on a Phenom Prox and by field-emission scanning electron microscopy (Ultra 55, Zeiss, Germany) with an acceleration voltage of 20.0 kV. X-ray photoelectron spectroscopy (XPS) measurements were conducted on a Perkin-Elmer PHI 5000C spectrometer (Perkin-Elmer, Boston, MA, USA) using Mg K_α radiation ($h\nu$ = 1253.6 eV) as the excitation source. The C_{1s} peak at 284.6 eV was used as the reference of the binding energy. The N_2 adsorption isotherms were measured on a Micromeritics ASAP 2000 instrument (Micromeritics, Atlanta, GA, USA) at −196 °C. Specific surface areas of the catalysts were calculated by BET method and pore volumes were calculated by one-point method. Thermogravimetric (TG) analysis was carried out on a thermal analyzer TGA8000 (Perkin-Elmer, Waltham, MA, USA) under the inflow of air, with a ramp rate of 10 °C/min from 20–900 °C.

3.3. Basicity Measurement

The surface density of base sites was evaluated by neutralization titration. Typically, a 20 mg sample was put into 10 mL 0.05 mol/L aqueous hydrochloric acid solution. The mixture was stirred for 30 min under N_2 flow. The solid was then removed by filtration and the remaining solution was immediately titrated with a 0.05 mol/L sodium hydroxide solution using phenolphthalein as the indicator.

3.4. Catalyst Evaluation

Knoevenagel condensation. In a round bottom flask, 1 mmol benzaldehyde, 2 mmol malononitrile, 10 mL N,N-dimethylformamide, and 50 mg catalyst were added in this order and stirred at 60 °C for 0.5 h with reflux. The reaction products were analyzed using a GC9560 gas chromatograph equipped with a SE-30 capillary column (30 m × 0.25 mm × 0.3 μm).

Oxidation of benzyl alcohol. 0.1 g catalyst, 0.25 mmol benzyl alcohol, and 20 mL N,N-dimethylformamide were added into a round-bottom flask. The mixture was reacted at 80 °C for 3 h with an O_2 stream of 50 mL/min under magnetic stirring. The products were analyzed using a GC9560 gas chromatograph equipped with a SE-30 capillary column (30 m × 0.25 mm × 0.3 μm).

Oxidation–condensation tandem reaction. The tandem reaction of benzyl alcohol and malononitrile was carried out in a round-bottom flask equipped with a reflux condenser under magnetic stirring. Typically, 0.1 g catalyst was added into the mixture of 0.25 mmol benzyl alcohol, 0.5 mmol malononitrile, and 20 mL N,N-dimethylformamide. The reaction was performed at 80 °C for 3 h and 6 h, with an O_2 flow of 50 mL/min. Products were analyzed using a GC9560 gas chromatograph equipped with a SE-30 capillary column (30 m × 0.25 mm × 0.3 μm).

4. Conclusions

A bifunctional catalyst was prepared by supporting cobalt oxide on s-triazine-based carbon nitride. The abundant ammonia species (especially –NH and $–NH_2$ groups) on the support not only act as basic active sites for Knoevenagel condensation but also enhance the catalytic activity of Co species in oxidation reactions. This catalyst exhibits excellent catalytic performance in the aerobic oxidation–Knoevenagel condensation tandem reaction without any auxiliary reagent and can easily be reused by simple filtration, for which the activity reduces by only 11.5% after four circles. The catalyst has fantastic potential for applications in industrial production.

Supplementary Materials: The following are available online at http://www.mdpi.com/2073-4344/10/6/712/s1: Figure S1: N_2 adsorption/desorption isotherms of (a) tri-g-C_3N_4, (b) 1CoO_x/tri-g-C_3N_4, (c) 3CoO_x/tri-g-C_3N_4, (d) 5CoO_x/tri-g-C_3N_4, and (e) 7CoO_x/tri-g-C_3N_4. Figure S2: XPS spectra of Co_{2p} in the 1CoO_x/tri-g-C_3N_4, 3CoO_x/tri-g-C_3N_4, 5CoO_x/tri-g-C_3N_4, and 7CoO_x/tri-g-C_3N_4. Figure S3: XPS spectra of O_{1s} in the 1CoO_x/tri-g-C_3N_4, 3CoO_x/tri-g-C_3N_4, 5CoO_x/tri-g-C_3N_4, and 7CoO_x/tri-g-C_3N_4.

Author Contributions: Y.Y. conceived and designed the experiments; J.W. performed the experiments; Y.Y., W.H., and Z.G. analyzed the data; J.W. wrote the original draft; W.H. and Y.Y. revised the paper. All authors have read and agreed to the published version of the manuscript.

Funding: This research was funded by the National Natural Science Foundation of China, grant number 91645201 and 21273043, National Key R&D Program of Ministry of Science and Technology, grant number 2017YFB0602204 and the Science & Technology Commission of Shanghai Municipality (19DZ2270100).

Conflicts of Interest: The authors declare no conflict of interest.

References

1. Corma, A.; Rodenas, T.; Sabater, M.J. Monoalkylations with alcohols by a cascade reaction on bifunctional solid catalysts: Reaction kinetics and mechanism. *J. Catal.* **2011**, *279*, 319–327. [CrossRef]
2. Li, P.; Cao, C.Y.; Chen, Z.; Liu, H.; Yu, Y.; Song, W.G. Core-shell structured mesoporous silica as acid-base bifunctional catalyst with designated diffusion path for cascade reaction sequences. *Chem. Commun.* **2012**, *48*, 10541–10543. [CrossRef] [PubMed]

3. Liu, P.; Li, C.; Hensen, E.J. Efficient tandem synthesis of methyl esters and imines by using versatile hydrotalcite-supported gold nanoparticles. *Chem. Eur. J.* **2012**, *18*, 12122–12129. [CrossRef] [PubMed]
4. Yang, H.; Fu, L.; Wei, L.; Liang, J.; Binks, B.P. Compartmentailzation of incompatible reagents within pickering emulsion droplets for one-pot cascade reactions. *J. Am. Chem. Soc.* **2015**, *137*, 1362–1371. [CrossRef] [PubMed]
5. Dhakshinamoorthy, A.; Garcia, H. Cascade reactiions catalyzed by metal organic frameworks. *ChemSusChem* **2014**, *7*, 2392–2410. [CrossRef]
6. Liu, K.; Xu, Y.; Yao, Z.; Miras, H.N.; Song, Y.F. Polyoxometalate-intercalated layered double hydroxides as efficient and recyclable bifunctional catalysts for cascade reactions. *ChemCatChem* **2016**, *8*, 929–937. [CrossRef]
7. Fernandes, A.E.; Riant, O.; Jensen, K.F.; Jonas, A.M. Molecular engineering of trifunctional supported catalysts for the aerobic oxidation of alcohols. *Angew. Chem. Int. Ed.* **2016**, *55*, 11044–11048. [CrossRef]
8. Shiju, N.R.; Alberts, A.H.; Khalid, S.; Brown, D.R.; Rothenberg, G. Mesoporous silica with site-isolated amine and phosphotungstic acid groups: A solid catalyst with tunable antagonistic functions for one-pot tandem reactions. *Angew. Chem. Int. Ed.* **2011**, *50*, 9615–9619. [CrossRef]
9. Krylov, I.B.; Terent'ev, A.O. Oxidative C-O coupling of benzylmalononitrile with 3-(hydroxyimino) pentane-2,4-dione. *J. Org. Chem.* **2015**, *51*, 10–13. [CrossRef]
10. Wang, J.S.; Jin, F.Z.; Ma, H.C.; Li, X.B.; Liu, M.Y.; Kan, J.L.; Chen, G.J.; Dong, Y.B. Au@Cu(II)-MOF: Highly efficient bifunctional heterogeneous catalyst for successive oxidation-condensation reactions. *Inorg. Chem.* **2016**, *55*, 6685–6691. [CrossRef]
11. Sarmah, B.; Srivastava, R.; Manjunathan, P.; Shanbhag, G.V. Green and sustainable tandem catalytic approach for fine-chemicals synthesis using octahedral MnO_2 molecular sieve: Catalytic activity versus method of catalyst synthesis. *ACS Sustain. Chem. Eng.* **2015**, *3*, 2933–2943. [CrossRef]
12. Xu, L.; Li, C.; Zhang, K.; Wu, P. Bifunctional tandem catalysis on multilamellar organic-inorganic hybrid zeolites. *ACS Catal.* **2014**, *4*, 2959–2968. [CrossRef]
13. Chen, C.; Yang, H.; Chen, J.; Zhang, R.; Guo, L.; Gan, H.; Song, B.; Zhu, W.; Hua, L.; Hou, Z. One-pot tandem catalytic synthesis of α,β-unsaturated nitriles from alcohol with nitriles in aqueous phase. *Catal. Commun.* **2014**, *47*, 49–53. [CrossRef]
14. Yang, Q.; Zhang, H.Y.; Wang, L.; Zhang, Y.; Zhang, Y.; Zhao, J. Ru/UiO-66 catalyst for the reduction of nitroarenes and tandem reaction of alcohol oxidation/Knoevenagel condensation. *ACS Omega* **2018**, *3*, 4199–4212. [CrossRef] [PubMed]
15. Sun, Q.; Aguila, B.; Ma, S. A bifunctional covalent organic framework as an efficient platform for cascade catalysis. *Mater. Chem. Front.* **2017**, *1*, 1310–1316. [CrossRef]
16. Qin, Y.; Luan, Y.; Peng, X.; Yang, M.; Hou, J.; Wang, G. Design and synthesis of an Au@MIL-53(NH_2) catalyst for a one-pot aerobic oxidation/Knoevenagel condensation reaction. *Eur. J. Inorg. Chem.* **2015**, *2015*, 5099–5105.
17. Miao, Z.; Luan, Y.; Qi, C.; Ramella, D. The synthesis of a bifunctional copper metal organic framework and its application in the aerobic oxidation/Knoevenagel condensation sequential reaction. *Dalton Trans.* **2016**, *45*, 13917–13924. [CrossRef]
18. Yan, H.; Zhang, H.Y.; Wang, L.; Zhang, Y.; Zhao, J. Ru(OH)x supported on polyethylenimine modified magnetic nanoparticles coated with silica as catalyst for one-pot tandem aerobic oxidation/Knoevenagel condensation of alcohols and active methylene compounds. *React. Kinet. Mech. Catal.* **2018**, *125*, 789–806. [CrossRef]
19. Wu, J.Q.; Hua, W.M.; Yue, Y.H.; Gao, Z. Swelling characteristics of g-C_3N_4 as base catalyst in liquid-phase reaction. *Acta Phys. Chim. Sin.* **2020**, *36*, 1904066. [CrossRef]
20. Zhao, Z.; Sun, Y.; Dong, F. Graphitic carbon nitride based nanocomposites: A review. *Nanoscale* **2015**, *7*, 15–37. [CrossRef]
21. Chan, M.; Liu, R.; Hsiao, M. Graphitic carbon nitride-based nanocomposites and their biological applications: A review. *Nanoscale* **2019**, *11*, 14993–15003. [CrossRef] [PubMed]
22. Rono, N.; Kibet, J.; Martincigh, B.; Nyamori, V. A review of the current status of graphitic carbon nitride. *Crit. Rev. Solid State Mater. Sci.* **2020**. [CrossRef]
23. Bai, C.; Li, A.; Yao, X.; Liu, H.; Li, Y. Efficient and selective aerobic oxidation of alcohols catalyzed by MOF-derived Co catalysts. *Green Chem.* **2016**, *18*, 1061–1069. [CrossRef]

24. Li, M.; Fu, X.; Peng, L.; Bai, L.; Wu, S.; Kan, Q.; Guan, J. Synthesis of three-dimensional-ordered mesoporous cobalt oxides for selective oxidation of benzyl alcohol. *ChemistrySelect* **2017**, *2*, 9486–9489. [CrossRef]
25. Cordoba, M.; Miranda, C.; Lederhos, C.; Pascual, F.C.; Ardila, A.; Fuentes, G.A.; Pouilloux, Y.; Ramirez, A. Catalytic performance of Co_3O_4 on different activated carbon supports in the benzyl alcohol oxidation. *Catalysts* **2017**, *7*, 384. [CrossRef]
26. Zhu, J.; Kailasam, K.; Fischer, A.; Thomas, A. Supported cobalt oxide nanoparticles as catalyst for aerobic oxidation of alcohols in liquid phase. *ACS Catal.* **2011**, *1*, 342–347. [CrossRef]
27. Wu, J.; Hua, W.; Yue, Y.; Gao, Z. g-C_3N_4 modified Co_3O_4 as efficient catalysts for aerobic oxidation of benzyl alcohol. *React. Kinet. Mech. Catal.* **2019**, *128*, 109–120. [CrossRef]
28. Shojaei, F.; Kang, H. Stability and electronic structures of triazine-based carbon nitride nanotubes. *RSC Adv.* **2015**, *5*, 10892–10898. [CrossRef]
29. Zhu, W.; Song, H.; Lv, Y. Triazine-based graphitic carbon nitride: Controllable synthesis and enhanced cataluminescent sensing for formic acid. *Anal. Bioanal. Chem.* **2018**, *410*, 7499–7509. [CrossRef]
30. Zhu, B.; Wageh, S.; Al-Ghamdi, A.; Yang, S.; Tian, Z.; Yu, J. Adsorption of CO_2, O_2, NO and CO on s-triazine-based g-C_3N_4 surface. *Catal. Today* **2019**, *335*, 117–127. [CrossRef]
31. Wang, H.; Wang, Y.; Guo, Y.; Ren, X.K.; Wu, L.; Liu, L.; Shi, Z.; Wang, Y. Pd nanoparticles confined within triazine-based carbon nitride NTs: An efficient catalyst for Knoevenagel condensation-reduction cascade reactions. *Catal. Today* **2019**, *330*, 124–134. [CrossRef]
32. Yang, J.; Liang, Y.; Li, K.; Yang, G.; Wang, K.; Xu, R.; Xie, X. One-step synthesis of novel K^+ and cyano groups decorated triazine-/heptazine-based g-C_3N_4 tubular homojunctions for boosting photocatalytic H_2 evolution. *Appl. Catal. B Environ.* **2020**, *262*, 118252. [CrossRef]
33. Liotta, L.F.; Cario, G.D.; Pantaleo, G.; Venezia, A.M.; Deganello, G. Co_3O_4/CeO_2 composite oxides for methane emissions abatement: Relationship between Co_3O_4–CeO_2 interaction and catalytic activity. *Appl. Catal. B Environ.* **2006**, *66*, 217–227. [CrossRef]
34. Petitto, S.C.; Marsh, E.M.; Carson, G.A.; Langell, M.A. Cobalt oxide surface chemistry: The interaction of CoO(100), Co_3O_4(110) and Co_3O_4(111) with oxygen and water. *J. Mol. Catal. A Chem.* **2008**, *281*, 49–58. [CrossRef]
35. Zhang, F.; Jiang, H.Y.; Li, X.Y.; Wu, X.T.; Li, H.X. Amine-functionalized GO as an active and reusable acid–base bifunctional catalyst for one-pot cascade reactions. *ACS Catal.* **2014**, *4*, 394–401. [CrossRef]
36. Xia, Y.; Dai, H.; Jiang, H.; Zhang, L. Three-dimensional ordered mesoporous cobalt oxides: Highly active catalysts for the oxidation of toluene and methanol. *Catal. Commun.* **2010**, *11*, 1171–1175. [CrossRef]
37. Lee, K.J.; Kumar, P.A.; Maqbool, M.S.; Rao, K.N.; Song, K.H.; Ha, H.P. Ceria added Sb-V_2O_5/TiO_2 catalysts for low temperature NH_3 SCR: Physic-chemical properties and catalytic activity. *Appl. Catal. B Environ.* **2013**, *142*, 705–717. [CrossRef]
38. Kang, M.; Park, E.D.; Kim, J.M.; Yie, J.E. Manganese oxide catalysts for NO_x reduction with NH_3 at low temperature. *Appl. Catal. A Gen.* **2007**, *327*, 261–269. [CrossRef]
39. Slot, T.K.; Eisenberg, D.; van Noordenne, D.; Jungbacker, P.; Rothenberg, G. Cooperative catalysis for selective alcohol oxidation with molecular oxygen. *Chem. Eur. J.* **2016**, *22*, 12307–12311. [CrossRef]
40. Mo, X.H.; Lopez, D.E.; Suwannakarn, K.; Liu, Y.; Lotero, E.; Goodwin, J.G., Jr.; Lu, C. Activation and deactivation characteristics of sulfonated carbon catalysts. *J. Catal.* **2008**, *254*, 332–338. [CrossRef]
41. Luo, D.; Liu, S.; Liu, J.; Zhao, J.; Miao, C.; Ren, J. Catalytic combustion of toluene over cobalt oxides supported on graphitic carbon nitride (CoO_x/g-C_3N_4) catalyst. *Ind. Eng. Chem. Res.* **2018**, *57*, 11920–11928. [CrossRef]
42. Xu, L.; Wang, Z.; Wang, J.; Xiao, Z.; Huang, X.; Liu, Z.; Wang, S. N-doped nanoporous Co_3O_4 nanosheets with oxygen vacancies as oxygen evolving electrocatalysts. *Nanotechnology* **2017**, *28*, 165402. [CrossRef] [PubMed]
43. Christoskova, S.G.; Stojanova, M.; Georgieva, M.; Mehandzhiey, D. Study on the thermal stability of a high Co-oxide used as low-temperature catalyst and oxidant for complete oxidation. *Thermochim. Acta* **1997**, *292*, 77–83. [CrossRef]